Proceedings of the Eighteenth International Conference on
Civil, Structural and Environmental Engineering Computing
Edited by: P. Iványi, J. Kruis and B.H.V. Topping
Civil-Comp Conferences, Volume 10, Paper 4.3
Civil-Comp Press, Edinburgh, United Kingdom, 2025
ISSN: 2753-3239, doi: 10.4203/ccc.10.4.3

Size Optimization of Beam Structures With Respect to Self-Weight

T. Světlík and M. Čermák

Department of mathematics, VSB-TUO, Ostrava, Czechia

Abstract

This paper investigates the size optimization of beam structures under self-weight loading. The study formulates a gradient-based optimization framework incorporating first-order sensitivity analysis of both the objective function and constraints. A key challenge arises from the nonlinear dependence of critical internal forces on cross-sectional geometry. Two formulations of the ultimate limit state strength constraints are compared: a bounded format, which directly limits internal forces, and a relative format, which expresses constraints as ratios of internal forces to resistances. The paper provides full analytical derivatives for both formats, emphasizing their linearization properties. The proposed methodology is tested on both statically determinate and indeterminate structures, enabling a systematic evaluation of constraint behavior, convergence robustness, and computational efficiency. Results show that while the bounded format offers better constraint control for large sections, it may cause infeasibility near small designs. Conversely, the relative format improves robustness across a wider design space. The findings highlight important trade-offs between formulation styles and provide guidance for selecting constraint formats in self-weight-dominated structural optimization problems.

Keywords: structural optimization, size optimization, self-weight, beam structures, inexact restoration, nonlinear programming

1 Introduction

Minimizing structural weight is a fundamental objective in engineering fields such as civil, aerospace, and mechanical engineering [7] [6]. In beam structures, this task becomes particularly challenging due to the influence of self-weight [5]. Unlike externally applied loads, self-weight is directly dependent on the structure's geometry and material properties, creating an intrinsic link between the load and the design variables. This coupling introduces a unique layer of complexity, making size optimization under self-weight a distinct and demanding subclass of structural optimization.

The goal is to minimize the total weight of the structure while satisfying key performance criteria, including strength, stiffness, deflection limits, buckling [9] resistance, and others [12]. Both the objective function and the constraints often involve nonlinear, non-convex relationships, increasing the mathematical and computational demands of the problem.

To address these challenges efficiently, gradient-based optimization methods are typically preferred. While metaheuristic algorithms can explore the design space globally [2], they are often too computationally intensive for iterative design processes that require rapid feedback. In contrast, well-established techniques such as sequential quadratic programming [4], Interior Point Methods, and the Method of Moving Asymptotes [10] are widely adopted for their fast convergence and ability to handle continuous, constrained problems effectively.

Among these, the Inexact Restoration (IR) method [8] [11] offers a compelling alternative. Its strength lies in a two-phase framework that decouples feasibility and optimality. The feasibility phase focuses on satisfying critical constraints—such as structural equilibrium and compatibility—while the optimality phase targets objective function reduction. This separation allows greater algorithmic flexibility and robustness, especially when dealing with complex or computationally intensive constraint sets. Moreover, under standard assumptions, IR ensures convergence to a stationary point.

The design variables typically describe geometric quantities such as cross-sectional area, moment of inertia, height, and width. Constraints are formulated based on performance criteria, including allowable stresses, displacement limits, and stability conditions. Since self-weight is a function of the design itself, any modification to these variables simultaneously alters both the applied loads and the structural response. This strong interdependence underscores the necessity for optimization strategies that can handle the mutual influence of objectives and constraints in a tightly integrated, iterative manner.

The remainder of the paper is organized as follows: Section 2 formulates the weight optimization problem and design constraints; Section 3 presents the finite element analysis; Section 4 discusses the strength constraints; Section 5 compares two constraint formulations; Section 6 derives a fully analytical sensitivity analysis; Section 7 demonstrates the approach on numerical benchmarks; and Section 8 concludes with key findings.

2 Weight optimisation

The goal of structural weight optimization is to minimize the total weight of the structure while satisfying geometric and mechanical constraints. In this work, we consider a beam structure with fixed geometry, where all members share identical cross-sectional and material properties along their length. For simplicity, and to isolate the effect of self-weight, all members are assumed to have the same cross-section. However, the proposed methodology can be extended to allow individual cross-section optimization for each member, at the cost of introducing additional design variables.

Under this assumption, the total structural weight $m(\mathbf{a})$ is given by

$$m(\mathbf{a}) := A(\mathbf{a}) \sum_{i=1}^{n_e} l_i \rho_i, \tag{1}$$

where $\mathbf{a} \in \mathbb{R}^{n_p}$ is the vector of geometric parameters, $A(\mathbf{a})$ is the cross-sectional area, $l_i > 0$ and $\rho_i > 0$ denote the length and material density of the i-th member, respectively, and n_e is the total number of members.

The vector $\mathbf{a}$ encodes the geometric properties of the cross-section. The number of parameters n_p depends on the selected cross-section type and its parametric model. For instance, square and circular sections are often described by a single parameter, while rectangular and pipe sections require two. More complex profiles, such as I-shaped sections, may require four to six parameters.

To ensure physically meaningful designs, the geometric parameters are subject to a set of inequality constraints:

$$\mathbf{c}_g(\mathbf{a}) \leq \mathbf{o}, \tag{2}$$

where $\mathbf{c}_g(\mathbf{a}) \in \mathbb{R}^{n_g}$ is the vector of n_g geometric constraints, and $\mathbf{o}$ is the zero vector of appropriate dimension. These constraints enforce both lower and upper bounds on each parameter and may also include relationships between them. For example, in a rectangular section, both width $b \in \mathbb{R}$ and height $h \in \mathbb{R}$ must be strictly positive e.g.

$$A(b, h) = bh \tag{3}$$

$$0 \leq b_{\min} \leq b, \quad 0 \leq h_{\min} \leq h \tag{4}$$

Such conditions are essential to exclude non-physical or impractical designs.

The geometric optimization problem can thus be formulated as

$$\begin{aligned} \min_{\mathbf{a} \in \mathbb{R}^{n_p}} \quad & m(\mathbf{a}) \\ \text{subject to} \quad & \mathbf{c}_g(\mathbf{a}) \leq \mathbf{0}. \end{aligned} \tag{5}$$

Since the vector $\mathbf{a}$ typically governs thicknesses or component dimensions, minimizing $m(\mathbf{a})$ naturally drives the solution toward the zero vector. This corresponds to a vanishing cross-sectional area and a structure with negligible weight, which is physically meaningless.

To obtain meaningful designs, additional constraints related to structural performance must be imposed. These typically limit internal stresses, displacements, or other response quantities under loading. Since such responses depend nonlinearly on $\mathbf{a}$ and are rarely available in closed form, we evaluate them numerically using the finite element method (FEM) [3]. The resulting quantities are incorporated into the optimization problem as constraints ensuring strength, stiffness, and serviceability.

3 Structural analysis via FEM

The objective of structural optimization is to reduce the structure's weight while ensuring its strength and serviceability requirements are met. To assess structural behavior, we use the FEM, which solves the discretized total potential energy of the system. FEM is particularly well suited for the beam structures considered in this work, where all elements share uniform cross-sectional and material properties.

The structural equilibrium problem is formulated as the minimization of the total potential energy

$$\min_{\mathbf{r}\in\mathbb{R}^{n_d}} \quad \frac{1}{2}\mathbf{r}^\top \mathbf{K}(\mathbf{a})\mathbf{r} - \mathbf{r}^\top \mathbf{f}(\mathbf{a}), \tag{6}$$

which is equivalent to the linear system

$$\mathbf{K}(\mathbf{a})\mathbf{r} = \mathbf{f}(\mathbf{a}), \tag{7}$$

where $\mathbf{K}(\mathbf{a}) \in \mathbb{R}^{n_d \times n_d}$ is the symmetric positive-definite global stiffness matrix, $\mathbf{f}(\mathbf{a}) \in \mathbb{R}^{n_d}$ is the global load vector, and $\mathbf{r} \in \mathbb{R}^{n_d}$ is the vector of nodal displacements. The number of degrees of freedom is denoted by n_d, and both $\mathbf{K}(\mathbf{a})$ and $\mathbf{f}(\mathbf{a})$ depend on the geometric design vector $\mathbf{a}$. In this work, the terms displacement and force are used in a generalized sense. That is, displacement vectors include both translational displacements and rotations, while force vectors include both forces and moments.

The global stiffness matrix is assembled from elemental contributions

$$\mathbf{K}(\mathbf{a}) := \sum_{i=1}^{n_e} \mathbf{L}_i^\top \mathbf{T}_i^\top \mathbf{K}_{e,i}(\mathbf{a}) \mathbf{T}_i \mathbf{L}_i, \tag{8}$$

where $\mathbf{K}_{e,i} \in \mathbb{R}^{6\times 6}$ is the local stiffness matrix of element i, $\mathbf{T}_i \in \mathbb{R}^{6\times 6}$ is the transformation matrix from local to global coordinates, and $\mathbf{L}_i \in \mathbb{R}^{6\times n_d}$ is the boolean allocation matrix.

For 2D Euler–Bernoulli beam elements, the local stiffness matrix is given by

$$\mathbf{K}_{e,i}(\mathbf{a}) = A(\mathbf{a})\mathbf{K}_{e,T,i} + I(\mathbf{a})\mathbf{K}_{e,E,i}, \tag{9}$$

where $A(\mathbf{a})$ is the cross-sectional area and $I(\mathbf{a})$ is the second moment of area. The matrices $\mathbf{K}_{e,T,i}$ and $\mathbf{K}_{e,E,i}$ represent the contributions from axial deformation and bending, respectively, and are independent of the design variables $\mathbf{a}$ [3, 11].

As these matrices are constant with respect to the design variables, the local stiffness matrix $\mathbf{K}_{e,i}(\mathbf{a})$ depends solely on the geometric quantities $A(\mathbf{a})$ and $I(\mathbf{a})$.

Under the assumption of a single cross-section for all elements, the global stiffness matrix $\mathbf{K}(\mathbf{a})$ simplifies to

$$\mathbf{K}(\mathbf{a}) = \widehat{\mathbf{K}}(\mathbf{a}) := A(\mathbf{a})\widehat{\mathbf{K}}_T + I(\mathbf{a})\widehat{\mathbf{K}}_E. \tag{10}$$

where

$$\widehat{\mathbf{K}}_T := \sum_{i=1}^{n_e} \mathbf{L}_i^\top \mathbf{T}_i^\top \mathbf{K}_{e,T,i} \mathbf{T}_i \mathbf{L}_i, \quad \widehat{\mathbf{K}}_E := \sum_{i=1}^{n_e} \mathbf{L}_i^\top \mathbf{T}_i^\top \mathbf{K}_{e,E,i} \mathbf{T}_i \mathbf{L}_i. \tag{11}$$

3.1 Load vector due to self-weight

The global load vector is similarly assembled from element contributions

$$\mathbf{f}(\mathbf{a}) := \sum_{i=1}^{n_e} \mathbf{L}_i^\top \mathbf{T}_i^\top \mathbf{f}_{\text{loc},i}(\mathbf{a}), \tag{12}$$

where $\mathbf{f}_{\text{loc},i}(\mathbf{a}) \in \mathbb{R}^6$ is the local load vector of the i-th element. This vector is defined as

$$\mathbf{f}_{\text{loc},i}(\mathbf{a}) := \mathbf{F}_{g,i} \mathbf{q}_{\text{loc},i}(\mathbf{a}), \tag{13}$$

with

$$\mathbf{F}_{g,i} := \begin{bmatrix} -l_i/2 & 0 \\ 0 & -l_i/2 \\ 0 & -l_i^2/12 \\ -l_i/2 & 0 \\ 0 & -l_i/2 \\ 0 & l_i^2/12 \end{bmatrix}, \quad \mathbf{q}_{\text{loc},i}(\mathbf{a}) := \begin{bmatrix} n_{\text{loc},i}(\mathbf{a}) \\ q_{\text{loc},i}(\mathbf{a}) \end{bmatrix}. \tag{14}$$

Here, $\mathbf{F}_{g,i} \in \mathbb{R}^{6\times 2}$ is the consistent load shape matrix that distributes axial and transverse loads to the element's nodal degrees of freedom. The vector $\mathbf{q}_{\text{loc},i}(\mathbf{a}) \in \mathbb{R}^2$ contains the distributed loads in the local coordinate system, where $n_{\text{loc},i}(\mathbf{a}) \in \mathbb{R}$ and $q_{\text{loc},i}(\mathbf{a}) \in \mathbb{R}$ denote the axial and transverse components, respectively.

Assuming gravity acts in the global vertical direction, the transverse component of self-weight in global coordinates is given by

$$q_i(\mathbf{a}) := A(\mathbf{a})\rho_i g, \tag{15}$$

where g is the gravitational acceleration. This load is then transformed into the local coordinate system as

$$\mathbf{q}_{\text{loc},i}(\mathbf{a}) := \mathbf{t}_i q_i(\mathbf{a}), \quad \mathbf{t}_i := \begin{bmatrix} \sin(\beta_i) \\ \cos(\beta_i) \end{bmatrix}, \tag{16}$$

where $\mathbf{t}_i \in \mathbb{R}^2$ is a direction vector that projects the vertical self-weight onto the local coordinate axes of the element, and β_i is the inclination angle of element i.

Substituting expressions (15) and (16) into (13), we obtain the simplified local load vector

$$\mathbf{f}_{\text{loc},i}(\mathbf{a}) = \hat{\mathbf{f}}_{\text{loc},i}(\mathbf{a}) := A(\mathbf{a})\rho_i g \mathbf{F}_{g,i}\mathbf{t}_i. \tag{17}$$

Inserting this into the global load vector expression (12) yields the compact form

$$\mathbf{f}(\mathbf{a}) = \hat{\mathbf{f}}(\mathbf{a}) := A(\mathbf{a})\hat{\mathbf{f}}_g, \tag{18}$$

where

$$\hat{\mathbf{f}}_g := \sum_{i=1}^{n_e} \rho_i g\, \mathbf{L}_i^\top \mathbf{T}_i^\top \mathbf{F}_{g,i}\mathbf{t}_i. \tag{19}$$

3.2 Internal force recovery

Since the global stiffness matrix $\mathbf{K}(\mathbf{a})$ is symmetric and positive definite, guaranteed by $\mathbf{c}_g(\mathbf{a})$, the displacement vector $\mathbf{r}$ has a unique solution for any given load vector. In particular, the displacement field is an implicit function of the design variables and is given by

$$\mathbf{r}(\mathbf{a}) = \mathbf{K}^{-1}(\mathbf{a})\,\mathbf{f}(\mathbf{a}), \tag{20}$$

Once the displacements are known, the nodal forces in each element can be computed as

$$\mathbf{f}_{e,i}(\mathbf{a}) = \begin{bmatrix} N_{1,i}(\mathbf{a}) \\ V_{1,i}(\mathbf{a}) \\ M_{1,i}(\mathbf{a}) \\ N_{2,i}(\mathbf{a}) \\ V_{2,i}(\mathbf{a}) \\ M_{2,i}(\mathbf{a}) \end{bmatrix} := \mathbf{K}_{e,i}(\mathbf{a})\,\mathbf{T}_i\mathbf{L}_i\,\mathbf{r}(\mathbf{a}) + \hat{\mathbf{f}}_{\text{loc},i}(\mathbf{a}), \tag{21}$$

where $\mathbf{f}_{e,i}(\mathbf{a}) \in \mathbb{R}^6$ contains the axial forces $N_{1,i}$, $N_{2,i}$, shear forces $V_{1,i}$, $V_{2,i}$, and bending moments $M_{1,i}$, $M_{2,i}$ at the start and end nodes of element i.

For elements subjected to distributed self-weight, the internal force distributions along the element are given by

$$N_i(\mathbf{a}, x_i) = N_{1,i}(\mathbf{a}) - n_{\text{loc},i}(\mathbf{a})\, x_i, \tag{22}$$

$$V_i(\mathbf{a}, x_i) = V_{1,i}(\mathbf{a}) - q_{\text{loc},i}(\mathbf{a})\, x_i, \tag{23}$$

$$M_i(\mathbf{a}, x_i) = M_{1,i}(\mathbf{a}) + V_{1,i}(\mathbf{a})\, x_i - \frac{q_{\text{loc},i}(\mathbf{a})}{2}\, x_i^2, \tag{24}$$

where $x_i \in [0, l_i]$ is the distance from the first node,

The axial force and shear force vary linearly along the element, with their extreme values occurring at the element nodes. In contrast, the bending moment exhibits a quadratic distribution and typically reaches its maximum at an interior point. This critical point is obtained by differentiating the moment function with respect to x_i and solving

$$x_{\text{crit},i}(\mathbf{a}) = \frac{V_{1,i}(\mathbf{a})}{q_{\text{loc},i}(\mathbf{a})}. \tag{25}$$

Substituting this value into the moment expression yields the critical bending moment

$$M_{\text{crit},i}(\mathbf{a}) := M_i(\mathbf{a}, x_{\text{crit},i}) = M_{1,i}(\mathbf{a}) + V_{1,i}(\mathbf{a})\, x_{\text{crit},i}(\mathbf{a}) - \frac{q_{\text{loc},i}(\mathbf{a})}{2}\, x^2_{\text{crit},i}(\mathbf{a}). \quad (26)$$

Each of the internal forces computed from the finite element analysis is subsequently evaluated against its corresponding resistance function, ensuring that the cross-section provides adequate capacity to withstand both self-weight and any additional applied loading.

4 Structural resistance constraints

To ensure structural safety under the ultimate limit state (ULS), the internal forces in each element must not exceed the corresponding resistance capacities of the cross-section. Strength verification is carried out for axial force, shear force, and bending moment, based on the internal force distributions obtained from the finite element analysis.

The resistance of element i is characterized by three functions: axial resistance $N_{\text{Rd},i}(\mathbf{a}) \geq 0$, shear resistance $V_{\text{Rd},i}(\mathbf{a}) \geq 0$, and bending resistance $M_{\text{Rd},i}(\mathbf{a}) \geq 0$. These functions are assumed to be nonnegative and depend solely on the cross-sectional geometry $\mathbf{a}$. They are considered known and reflect standard code-based strength criteria [1]. In this work, $N_{\text{Rd},i}(\mathbf{a})$, $V_{\text{Rd},i}(\mathbf{a})$, and $M_{\text{Rd},i}(\mathbf{a})$ represent the total design resistance, accounting for both material strength and stability effects, including buckling and lateral-torsional buckling.

From the finite element solution, the corresponding design internal forces are extracted for each element i, namely the axial force $N_{\text{Ed},i}(\mathbf{a})$, shear force $V_{\text{Ed},i}(\mathbf{a})$, and bending moment $M_{\text{Ed},i}(\mathbf{a})$, representing the most critical values relevant to ULS verification. For instance, $M_{\text{Ed},i}(\mathbf{a}) = M_{\text{crit},i}(\mathbf{a})$.

The resulting strength constraints for each element i are given by

$$|N_{\text{Ed},i}(\mathbf{a})| \leq N_{\text{Rd},i}(\mathbf{a}), \quad |V_{\text{Ed},i}(\mathbf{a})| \leq V_{\text{Rd},i}(\mathbf{a}), \quad |M_{\text{Ed},i}(\mathbf{a})| \leq M_{\text{Rd},i}(\mathbf{a}). \quad (27)$$

These scalar inequalities define the *bounded* format, where internal forces are directly compared to resistance values in absolute terms. To express these ULS conditions compactly, the element-wise constraints are assembled into a local constraint vector

$$\mathbf{c}_{\text{ULS},i}(\mathbf{a}) := \begin{bmatrix} |N_{\text{Ed},i}(\mathbf{a})| - N_{\text{Rd},i}(\mathbf{a}) \\ |V_{\text{Ed},i}(\mathbf{a})| - V_{\text{Rd},i}(\mathbf{a}) \\ |M_{\text{Ed},i}(\mathbf{a})| - M_{\text{Rd},i}(\mathbf{a}) \end{bmatrix} \leq \mathbf{0}, \quad (28)$$

and assembled globally as

$$\mathbf{c}_{\text{ULS}}(\mathbf{a}) := \begin{bmatrix} \mathbf{c}_{\text{ULS},1}(\mathbf{a}) \\ \vdots \\ \mathbf{c}_{\text{ULS},n_e}(\mathbf{a}) \end{bmatrix} \leq \mathbf{0}. \quad (29)$$

This constraint formulation defines the feasible design space with respect to strength, ensuring that the cross-section can resist all internal forces due to self-weight and applied loads.

5 Influence of constraint formulation

Consider a simply supported beam subjected only to its self-weight. For a square cross-section with side length $b \in \mathbb{R}$, the critical bending moment due to self-weight scales with the square of the cross-sectional dimension

$$M_{\text{crit}}(b) = c_1 b^2, \tag{30}$$

where $c_1 > 0$ is a constant independent of b. The bending resistance scales with the section modulus, which for a square cross-section behaves like

$$M_{\text{Rd}}(b) = c_2 b^3, \tag{31}$$

with $c_2 > 0$, also independent of b.

Imposing the bounded strength condition (27) yields

$$c_1 b^2 \leq c_2 b^3. \tag{32}$$

Assuming $c_1 = c_2 = 1$ for simplicity, this reduces to

$$f_B(b) := b^2 - b^3 \leq 0. \tag{33}$$

The feasible region defined by this inequality is illustrated in Figure 1. The function $f_B(b)$ increases for small values of b, attains a maximum near $b \approx 0.66$, and then decreases for $b > 0.66$. Consequently, in the region $b < 0.66$, the local gradient is positive, and linear approximations may misleadingly suggest that decreasing b improves feasibility. However, this direction leads toward smaller values of b, potentially violating the constraint as $b \to 0$.

This illustrates a common pitfall in nonlinear programming: although the original constraint $f_B(b) \leq 0$ is satisfied for $b \geq 1$, a naive gradient-based step taken near $b = 0.5$ may misinterpret the constraint's local behavior and drive the design into an infeasible region.

To mitigate this issue, the constraint $f_B(b)$ can be reformulated in the *relative* format. By normalizing with respect to the design capacity $M_{\text{Rd}}(b)$, we obtain

$$f_R(b) := \frac{b^2}{b^3} - 1 = \frac{1}{b} - 1 \leq 0. \tag{34}$$

This concept generalizes naturally to internal force constraints in structural optimization. Based on the bounded formulation (32), the relative format leads to

$$\frac{|N_{\text{Ed},i}(\mathbf{a})|}{N_{\text{Rd},i}(\mathbf{a})} - 1 \leq 0, \quad \frac{|V_{\text{Ed},i}(\mathbf{a})|}{V_{\text{Rd},i}(\mathbf{a})} - 1 \leq 0, \quad \frac{|M_{\text{Ed},i}(\mathbf{a})|}{M_{\text{Rd},i}(\mathbf{a})} - 1 \leq 0. \tag{35}$$

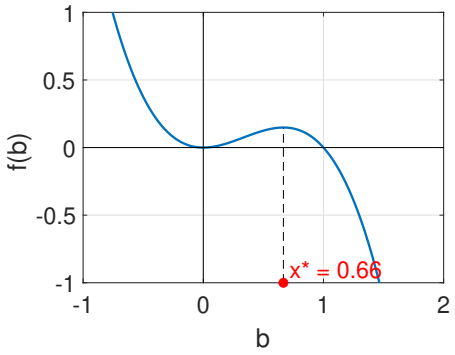

Figure 1: Bounded format constraint $f_B(b)$, with local maximum at $b \approx 0.66$.

Figure 2 compares the bounded and relative formulations. While both define the same feasible set, their analytical behavior differs markedly. As $b \to 0$, the relative constraint becomes increasingly steep, with unbounded gradients that may lead to numerical instability. Conversely, for large b, the constraint flattens and becomes nearly inactive, transferring optimization effort to other conditions, such as geometric constraints.

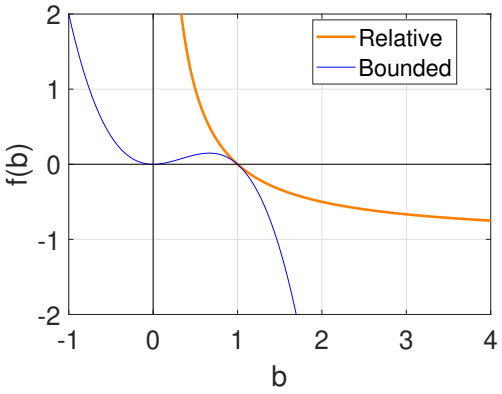

Figure 2: Comparison of constraint behavior for the bounded $f_B(b)$ and relative $f_R(b)$ formulations.

In contrast, the bounded formulation maintains constraint activity for large cross-sections, effectively penalizing over-design. However, it suffers near $b = 0$, where strong nonconvexity and vanishing gradients can impair linearization and misguide the search direction.

To assess implementation complexity, we compare the derivatives of the bounded (27) and the relative (35) constraint for axial force

$$\frac{\partial c_{\mathrm{B}}(\mathbf{a})}{\partial a_j} = \frac{\partial N_{\mathrm{Ed},i}(\mathbf{a})}{\partial a_j} - \frac{\partial N_{\mathrm{Rd},i}(\mathbf{a})}{\partial a_j}, \tag{36}$$

$$\frac{\partial c_{\mathrm{R}}(\mathbf{a})}{\partial a_j} = \frac{\dfrac{\partial N_{\mathrm{Ed},i}(\mathbf{a})}{\partial a_j} N_{\mathrm{Rd},i}(\mathbf{a}) - N_{\mathrm{Ed},i}(\mathbf{a}) \dfrac{\partial N_{\mathrm{Rd},i}(\mathbf{a})}{\partial a_j}}{N_{\mathrm{Rd},i}^2(\mathbf{a})}. \tag{37}$$

Both formats rely on the same underlying derivatives of internal forces and resistance functions. Therefore, their implementation cost is effectively equivalent. The choice between bounded and relative formulations can thus be guided by numerical behavior and optimization performance, rather than by derivative complexity.

6 Sensitivity analysis and gradient evaluation

Based on the structural model and strength constraints defined in the previous sections, the size optimization problem is now formulated as

$$\begin{aligned} \min_{\mathbf{a}} \quad & m(\mathbf{a}) \\ \text{subject to} \quad & \mathbf{c}(\mathbf{a}) \leq \mathbf{0}, \end{aligned} \tag{38}$$

where the constraint vector $\mathbf{c}(\mathbf{a}) \in \mathbb{R}^{n_c}$ groups together the geometric and strength-related conditions

$$\mathbf{c}(\mathbf{a}) = \begin{bmatrix} \mathbf{c}_g(\mathbf{a}) \\ \mathbf{c}_{\mathrm{ULS}}(\mathbf{a}) \end{bmatrix}. \tag{39}$$

To solve this nonlinear programming problem using gradient-based optimization, the constraints are linearized using first-order Taylor expansions around the current design iterate $\mathbf{a}_0 \in \mathbb{R}^{n_p}$. The j-th component of the constraint vector $\mathbf{c}(\mathbf{a})$, denoted $c_j(\mathbf{a})$, is approximated as

$$c_j(\mathbf{a}) \approx c_j(\mathbf{a}_0) + \nabla c_j(\mathbf{a}_0)^\top (\mathbf{a} - \mathbf{a}_0) \leq 0, \tag{40}$$

where the gradient $\nabla c_j(\mathbf{a}_0) \in \mathbb{R}^{n_p}$ contains the partial derivatives of $c_j(\mathbf{a})$ with respect to the design variables

$$\nabla c_j(\mathbf{a}) = \left[\frac{\partial c_j}{\partial a_1}, \quad \frac{\partial c_j}{\partial a_2}, \quad \cdots, \quad \frac{\partial c_j}{\partial a_{n_p}} \right]^\top. \tag{41}$$

Among all constraints, the most complex to linearize is the one involving the critical bending moment $M_{\text{crit},i}(\mathbf{a})$, defined in (26). This quantity depends nonlinearly on the internal forces $M_{1,i}(\mathbf{a})$, $V_{1,i}(\mathbf{a})$, the self-weight-induced load $q_{\text{loc},i}(\mathbf{a})$, and the critical location $x_{\text{crit},i}(\mathbf{a})$.

The derivative of $M_{\text{crit},i}$ with respect to the design variable a_j is given by:

$$\frac{\partial M_{\text{crit},i}(\mathbf{a})}{\partial a_j} = \frac{\partial M_{1,i}(\mathbf{a})}{\partial a_j} + \frac{\partial}{\partial a_j} \left(V_{1,i}(\mathbf{a})\, x_{\text{crit},i}(\mathbf{a}) \right) - \frac{1}{2} \frac{\partial}{\partial a_j} \left(q_{\text{loc},i}(\mathbf{a})\, x_{\text{crit},i}^2(\mathbf{a}) \right). \tag{42}$$

Using the product rule, the two remaining derivatives expand as

$$\frac{\partial}{\partial a_j} \left(V_{1,i}(\mathbf{a})\, x_{\text{crit},i}(\mathbf{a}) \right) = \frac{\partial V_{1,i}(\mathbf{a})}{\partial a_j} x_{\text{crit},i}(\mathbf{a}) + V_{1,i}(\mathbf{a}) \frac{\partial x_{\text{crit},i}(\mathbf{a})}{\partial a_j}, \tag{43}$$

$$\frac{\partial}{\partial a_j}\left(q_{\text{loc},i}(\mathbf{a})\, x^2_{\text{crit},i}(\mathbf{a})\right) = \frac{\partial q_{\text{loc},i}(\mathbf{a})}{\partial a_j} x^2_{\text{crit},i}(\mathbf{a}) + 2 q_{\text{loc},i}(\mathbf{a}) x_{\text{crit},i}(\mathbf{a}) \frac{\partial x_{\text{crit},i}(\mathbf{a})}{\partial a_j}. \tag{44}$$

The derivative of the critical location $x_{\text{crit},i}(\mathbf{a})$, from equation (25), is

$$\frac{\partial x_{\text{crit},i}(\mathbf{a})}{\partial a_j} = \frac{\dfrac{\partial V_{1,i}(\mathbf{a})}{\partial a_j} q_{\text{loc},i}(\mathbf{a}) - V_{1,i}(\mathbf{a}) \dfrac{\partial q_{\text{loc},i}(\mathbf{a})}{\partial a_j}}{q^2_{\text{loc},i}(\mathbf{a})}. \tag{45}$$

The shear force $V_{1,i}(\mathbf{a})$ and bending moment $M_{1,i}(\mathbf{a})$ are components of the internal nodal force vector $\mathbf{f}_{e,i}(\mathbf{a})$, computed using

$$\frac{\partial \mathbf{f}_{e,i}(\mathbf{a})}{\partial a_j} = \frac{\partial}{\partial a_j}\left(\mathbf{K}_{e,i}(\mathbf{a})\, \mathbf{T}_i\, \mathbf{L}_i\, \mathbf{r}(\mathbf{a})\right) + \frac{\partial \mathbf{f}_{\text{loc},i}(\mathbf{a})}{\partial a_j}. \tag{46}$$

Applying the chain rule to the stiffness-displacement product gives

$$\frac{\partial}{\partial a_j}\left(\mathbf{K}_{e,i}(\mathbf{a})\, \mathbf{T}_i\, \mathbf{L}_i\, \mathbf{r}(\mathbf{a})\right) = \frac{\partial \mathbf{K}_{e,i}(\mathbf{a})}{\partial a_j} \mathbf{T}_i \mathbf{L}_i\, \mathbf{r}(\mathbf{a}) + \mathbf{K}_{e,i}(\mathbf{a}) \mathbf{T}_i \mathbf{L}_i\, \frac{\partial \mathbf{r}(\mathbf{a})}{\partial a_j}. \tag{47}$$

The element stiffness matrix depends on cross-sectional area $A(\mathbf{a})$ and moment of inertia $I(\mathbf{a})$, via

$$\frac{\partial \mathbf{K}_{e,i}(\mathbf{a})}{\partial a_j} = \frac{\partial A(\mathbf{a})}{\partial a_j} \mathbf{K}_{e,T,i} + \frac{\partial I(\mathbf{a})}{\partial a_j} \mathbf{K}_{e,E,i}. \tag{48}$$

The derivative of self-weight load follows directly

$$\frac{\partial \mathbf{f}_{\text{loc},i}(\mathbf{a})}{\partial a_j} = \rho_i g\, \mathbf{F}_{g,i}\, \mathbf{t}_i \frac{\partial A(\mathbf{a})}{\partial a_j}. \tag{49}$$

The displacement vector $\mathbf{r}$ is obtained by solving the global system and differentiated as

$$\frac{\partial \mathbf{r}(\mathbf{a})}{\partial a_j} = \mathbf{K}^{-1}(\mathbf{a}) \left(\frac{\partial \hat{\mathbf{f}}(\mathbf{a})}{\partial a_j} - \frac{\partial \widehat{\mathbf{K}}(\mathbf{a})}{\partial a_j} \mathbf{r}(\mathbf{a}) \right), \tag{50}$$

where $\mathbf{K}^{-1}(\mathbf{a})$ is positive definite. The derivatives of the load and stiffness matrices are

$$\frac{\partial \hat{\mathbf{f}}}{\partial a_j} = \frac{\partial A}{\partial a_j} \mathbf{f}^{(1)} g, \tag{51}$$

$$\frac{\partial \widehat{\mathbf{K}}(\mathbf{a})}{\partial a_j} = \frac{\partial A(\mathbf{a})}{\partial a_j} \widehat{\mathbf{K}}_T + \frac{\partial I(\mathbf{a})}{\partial a_j} \widehat{\mathbf{K}}_E. \tag{52}$$

Despite the multiple steps involved, the linearized constraint (40) offers notable computational advantages. Since the constraint is evaluated at the current design iterate $\mathbf{a}_0$, the value $c_j(\mathbf{a}_0)$ is readily available. More importantly, many intermediate quantities, such as the displacement vector $\mathbf{r}(\mathbf{a}_0)$, internal element forces $\mathbf{f}_{e,i}(\mathbf{a}_0)$, and distributed loads, are already computed during this evaluation and can be efficiently

reused in assembling the gradient $\nabla c(\mathbf{a}_0)$. This reuse significantly reduces the computational overhead of gradient evaluation.

In addition, all components of the gradient are computed analytically, which enhances numerical accuracy and robustness compared to approximate methods like finite differences. Together, the reuse of intermediate results and the use of exact analytical derivatives ensure that the overall gradient evaluation remains both precise and computationally efficient.

7 Numerical benchmark

In the following numerical benchmarks, we examine the optimization behavior of structural members with rectangular cross-sections, parameterized by width and height ($n_p = 2$). The goal is to minimize total structural weight while satisfying ULS constraints. Both the bounded and relative formulations of the ULS conditions are investigated.

All simulations are carried out for structural steel with density $\rho = 7850\,\text{kg/m}^3$, Young's modulus $E = 210 \times 10^9\,\text{Pa}$, yield strength $f_y = 235 \times 10^6\,\text{Pa}$, and Poisson's ratio $\nu = 0.3$. The design checks include axial tension, compression, shear, and bending resistance, as well as in-plane buckling and lateral–torsional buckling, following the provisions of EN 1993-1-1 [1]. Resistance functions are defined for each beam element based on its geometry and loading and are applied consistently across both constraint formulations. All structural members are checked to ensure compliance with ULS criteria throughout the optimization.

To evaluate the behavior of each ULS formulation, we conduct optimization runs from multiple initial design points $\mathbf{a}_0$, ranging from undersized to oversized configurations. The initial designs are selected from the set $\mathbf{a}_0 \in [0.001, 1]\,\text{m}$, applied uniformly to all components of $\mathbf{a}_0$. For each case, we track the number of constraint evaluations, the number of linearizations, and overall convergence behavior, assessing the sensitivity of both formulations to the choice of starting point. All optimization problems are solved using the inexact restoration (IR) method. The implementation follows the framework described in [11], which provides robust performance for constrained nonlinear problems, especially when handling nonconvex or nonlinearly constrained formulations like those encountered in structural design.

7.1 Simply supported beam

The first benchmark considers a simply supported beam with a span of $l = 6\,\text{m}$, subjected to self-weight, as illustrated in Figure 3. The structure is statically determinate, meaning that the internal forces depend solely on geometry and loading, and are independent of cross-sectional stiffness.

The bending moment distribution follows a parabolic profile and reaches its maximum at midspan. In this configuration, the critical bending moment admits a closed-

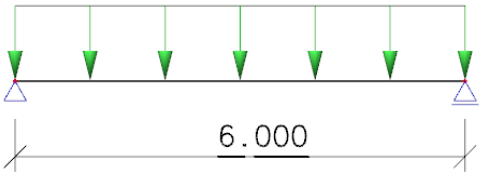

Figure 3: Simply supported beam of span 6 m, loaded by self-weight.

form analytical expression.

This benchmark serves as a minimal yet informative test case. It isolates the influence of self-weight in the optimization process, fully decoupled from stiffness-related effects. As such, it provides a clean setting for examining the numerical behavior of the bounded and relative ULS formulations under analytically tractable conditions.

The results of the optimization runs, reported in Table 1, summarize the number of constraint evaluations and linearizations for each formulation.

$\mathbf{a}_0$	**Bounded**		**Relative**	
[m]	Eval.	Lin.	Eval.	Lin.
0.001	Failed		32	22
0.0025	Failed		26	18
0.005	Failed		20	14
0.0075	Failed		17	12
0.01	Failed		14	10
0.025	12	7	16	11
0.05	15	8	34	23
0.075	20	11	34	23
0.1	22	12	34	23
0.25	28	15	34	23
0.5	32	17	34	23
0.75	34	18	36	24
1	34	18	36	24

Table 1: Convergence results for the simply supported beam. 'Eval.' = number of constraint evaluations, 'Lin.' = number of constraint linearization. The bounded formulation fails to converge for very small initial sizes (marked as Failed).

For initial designs with $\mathbf{a}_0 < 0.025$, the bounded formulation fails to converge. The linearized ULS constraints are locally infeasible in this region, as illustrated in Figure 1. In contrast, the relative formulation remains well-posed and converges reliably across the full range of initializations.

As the initial design size increases, the number of iterations required by the relative formulation also increases, but only up to a point. For sufficiently large $\mathbf{a}_0$, the ULS constraints become inactive due to high initial feasibility. The optimization is then governed primarily by geometric constraints. This behavior reflects the flattening of the relative constraint for large cross-sections, shown in Figure 2.

In such cases, the optimizer reduces the cross-section size rapidly. The resulting convergence behavior closely resembles that observed for small initial designs.

7.2 U-shaped structure

The second benchmark considers a U-shaped frame, subjected to self-weight, consisting of three rigidly connected segments: two vertical members and a horizontal base, as shown in Figure 4. The vertical legs are fixed at their upper ends, while the horizontal member spans $10\,\mathrm{m}$. The vertical heights of the legs are $3.6\,\mathrm{m}$ and $100.0\,\mathrm{m}$, respectively, creating a highly asymmetric frame with significant stiffness imbalance.

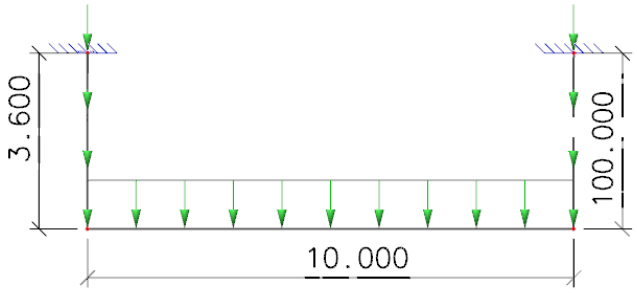

Figure 4: Asymmetric U-shaped frame with fixed supports at the top ends and uniformly distributed self-weight along the horizontal member. The configuration introduces stiffness-coupled load redistribution.

This configuration introduces structural indeterminacy, as the internal forces now depend on both the external loading and the relative stiffness of the members. Unlike the simply supported beam, the critical bending moment here is not known a priori—it emerges from the interaction between segments, and its location and magnitude are influenced by the geometric parameters of the cross-section. As such, both equilibrium and resistance become coupled to the design variables.

The indeterminate nature of the system creates additional challenges for optimization. Even though the applied load remains self-weight, its distribution through the structure depends on stiffness, making the structural response sensitive to cross-sectional changes. This benchmark therefore provides a more realistic and demanding test case, capturing the nonlinear behavior of ULS constraints in the presence of stiffness-induced load redistribution.

By comparing the bounded and relative formulations across a range of initial designs, we evaluate how each format handles stiffness-coupled sensitivities, local nonconvexities, and varying constraint activity throughout the optimization process. The results of these optimization runs—including the number of constraint evaluations and linearizations—are summarized in Table 2, providing a direct comparison of the computational behavior of both formulations.

In the U-shaped structure, a similar trend to the simply supported beam is observed. As $\mathbf{a}_0$ increases, the number of constraint evaluations and linearizations rises sharply.

The bounded formulation fails to converge for very small initial designs due to infeasible linearizations. However, it remains robust for larger initial values, though it typically requires more iterations than the relative formulation.

Near the optimal value around $\mathbf{a}_0 = 0.025$, the bounded formulation converges more quickly. It requires fewer linearizations than the relative approach, This highlights its potential efficiency when the initial design is well-scaled.

$\mathbf{a}_0$	**Bounded**		**Relative**	
[m]	Eval.	Lin.	Eval.	Lin.
0.001	Failed		47	26
0.0025	Failed		38	20
0.005	Failed		36	18
0.0075	Failed		33	16
0.01	Failed		19	13
0.025	21	14	33	17
0.05	27	17	49	27
0.075	32	20	49	27
0.1	38	24	49	27
0.25	37	22	49	27
0.5	53	32	49	27
0.75	92	57	51	28
1	117	70	51	28

Table 2: Convergence results for the U-shaped structure. 'Eval.' = number of constraint evaluations, 'Lin.' = number of constraint linearization. The bounded formulation fails to converge for very small initial sizes (marked as Failed).

8 Conclusion

This study examined the impact of self-weight and constraint formulation on the size optimization of beam structures under ULS criteria. A gradient-based optimization framework was developed using first-order constraint linearization, with full analytical sensitivity computation for both bounded and relative ULS constraint formats.

Two benchmark problems were considered: a simply supported beam with known analytical behavior and a statically indeterminate U-shaped frame where stiffness influences internal force redistribution. Across a range of initial designs, the numerical performance of both constraint formats was evaluated in terms of convergence behavior, constraint activity, and computational efficiency.

The results highlight a key trade-off between the two formulations. The bounded format maintains strong constraint gradients for large, over-designed sections, but suffers from nonconvexity and poor linearization near undersized configurations. Conversely, the relative format exhibits more consistent behavior near optimal designs

and avoids local infeasibility, but can become inactive in oversized regimes due to vanishing gradients.

Despite having similar implementation costs, the two formulations exhibit distinct numerical characteristics. The choice between them should be guided by the expected design regime and optimization robustness requirements. For problems dominated by self-weight and geometry-sensitive responses, the relative format offers a more reliable convergence path, while the bounded format may better maintain constraint activity in large-scale designs.

Acknowledgements

The work was supported by the Student Grant Competition of VŠB-TUO. The project registration number is SP2025/058.

Declaration of generative AI and AI-assisted technologies in the writing process.

During the preparation of this work, the authors used OpenAI's ChatGPT in order to assist with language refinement and improving the clarity and readability of the text. After using this tool, the authors reviewed and edited the content as needed and takes full responsibility for the content of the publication.

References

[1] EN 1993-1-1: Eurocode 3: Design of steel structures – Part 1-1: General rules and rules for buildings, 2005. European Committee for Standardization, Brussels.

[2] Mohamad Faiz Ahmad, Nor Ashidi Mat Isa, Wei Hong Lim, and Koon Meng Ang. Differential evolution: A recent review based on state-of-the-art works. *Alexandria Engineering Journal*, 61(5):3831–3872, May 2022.

[3] K.J. Bathe. *Finite Element Procedures*. Prentice Hall, 2006.

[4] Z. Dostál. *Optimal Quadratic Programming Algorithms, with Applications to Variational Inequalities*, volume 23. SOIA, Springer, New York, US, 2009.

[5] Helen E. Fairclough and Matthew Gilbert. Layout optimization of long-span structures subject to self-weight and multiple load-cases. *Structural and Multidisciplinary Optimization*, 65(7), June 2022.

[6] Robert Jankowski, Ahmed Manguri, Hogr Hassan, and Najmadeen Saeed. Topology, size, and shape optimization in civil engineering structures: A review. *Computer Modeling in Engineering & Sciences*, 142(2):933–971, 2025.

[7] János LÓGÓ and Hussein ISMAIL. Milestones in the 150-year history of topology optimization: A review, 2020.

[8] J. M. Martínez and E. A. Pilotta. Inexact-restoration algorithm for constrained optimization1. *Journal of Optimization Theory and Applications*, 104(1):135–163, January 2000.

[9] Florian Mitjana, Sonia Cafieri, Florian Bugarin, Christian Gogu, and Fabien Castanie. Optimization of structures under buckling constraints using frame elements. *Engineering Optimization*, 51(1):140–159, March 2018.

[10] K. Svanberg. The method of moving asymptotes—a new method for structural optimization. *International Journal for Numerical Methods in Engineering*, 24(2):359–373, February 1987.

[11] T. Světlík, M. Mrovec, L. Pospíšil, and M. Cermak. Size optimisation of 2d frame structures using inexact restoration. In *Proceedings of the Fifteenth International Conference on Computational Structures Technology*, volume 9 of *CST 2024*, page 1–13. Civil-Comp Press.

[12] Marek Tyburec, Michal Kočvara, Marouan Handa, and Jan Zeman. Global weight optimization of frame structures under free-vibration eigenvalue constraints, 2024.